SOUTHERN PLAINS
TRANSPORTATION CENTER

Temperature Effects in Bridge Condition Evaluation and Capacity Rating in Oklahoma

Jun He
Naiyu Wang, Ph.D.
K.K. Muraleetharan, Ph.D., P.E.

SPTC14.2-21-F

Southern Plains Transportation Center
201 Stephenson Parkway, Suite 4200
The University of Oklahoma
Norman, Oklahoma 73019

DISCLAIMER

The contents of this report reflect the views of the authors, who are responsible for the facts and accuracy of the information presented herein. This document is disseminated under the sponsorship of the Department of Transportation University Transportation Centers Program, in the interest of information exchange. The U.S. Government assumes no liability for the contents or use thereof.

1. Report No. SPTC14.2-21	2. Government Accession No.	3. Recipient's Catalog No.	
4. Title and Subtitle Temperature Effects in Bridge Condition Evaluation and Capacity Rating in Oklahoma		5. Report Date 11/23/2019	
		6. Performing Organization Code	
7. Author(s) Jun He; Naiyu Wang; K.K. "Muralee" Muraleetharan		8. Performing Organization Report No.	
9. Performing Organization Name and Address The University of Oklahoma Norman, OK 73019		10. Work Unit No. (TRAIS)	
		11. Contract or Grant No. DTRT13-G-UTC36	
12. Sponsoring Agency Name and Address Southern Plains Transportation Center 201 Stephenson Pkwy, Suite 4200 The University of Oklahoma Norman, OK 73019		13. Type of Report and Period Covered Final; May 2017 – November 2019	
		14. Sponsoring Agency Code	
15. Supplementary Notes			

16. Abstract

Spatial and temporal temperature variations in bridge structures due to changes in the surrounding climate produce movements which, if restrained, may induce stresses in the structure. Temperature effects have always been considered to be one of the critical issues that affect the performance of traditional PC bridges. Numerical and analytical studies were conducted on PC girder bridges in Oklahoma in order to (1) develop an efficient temperature loading model for predicting bridge temperature-induced response; and (2) develop guidelines to incorporate the effects of thermal actions in reliability-based condition evaluation.

17. Key Words Temperature, bridge condition, evaluation, capacity rating		18. Distribution Statement No restrictions. This publication is available at www.sptc.org and from the NTIS.	
19. Security Class. (of this report) Unclassified	20. Security Class. (of this page) Unclassified	21. No. of Pages 56	22. Price

TEMPERATURE EFFECTS IN BRIDGE CONDITION EVALUATION AND CAPACITY RATING IN OKLAHOMA

Final Report
2019.11.23

Jun He, Ph.D.
Naiyu Wang, Ph.D.
K.K. "Muralee" Muraleetharan, Ph.D.

Southern Plains Transportation Center
201 Stephenson Pkwy, Suite 4200
The University of Oklahoma
Norman, OK 73019

Table of Contents

List of Figures

List of Tables

Executive Summary

Oklahoma's climate ranges from humid subtropical in the east to semi-arid in the west. While summers are long and usually quite hot, periods of extreme cold during the winter months are infrequent. Normal daily mean temperatures in Oklahoma range from 37°F (3°C) in January to 82°F (28°C) in July. The record low temperature of –27°F (–33°C) was set in Watts on January 18, 1930; the record high, 120°F (49°C), occurred in Tipton on June 27, 1994. Extremes in temperatures may worsen as a result of climate change.

The effects of daily and seasonal temperature variations acting on the structural elements of a bridge system depend on bridge geometry, location and orientation, material properties and local weather conditions. Nonlinear temperature distributions through key structural elements of a bridge can be caused by the relatively low thermal conductivity of concrete construction materials and by the temporal and spatial variation of ambient temperature. For statically indeterminate or geometrically skewed bridges, this temperature variation may induce stresses in bridge spans that represent a significant percentage of the direct stress capacity of the bridge, determined as per the AASHTO LRFD Bridge Design Specifications (2012), and may lead to unacceptable performance in service.

The effects of temperature in bridge design traditionally have been accounted for by allowing for differential movement, e.g., expansion and contraction at bearings and joints. Temperature induced stresses are, however, rarely considered in any detail in bridge condition evaluation and capacity rating practice. With the increasing number of more complex and longer-span bridges being constructed in Oklahoma, where temperature ranges in excess of 100 °F may be observed over the course of a year, a better understanding and more accurate consideration of thermal loading effects should be reflected in bridge evaluation and rating methodologies.

This research develops a method to incorporate the effects of self-straining thermal actions, where necessary, in reliability-based condition evaluation and capacity rating of bridges in Oklahoma.

1 Introduction

Bridge structures are regularly subjected to significant temperature variations affected by complex interactions of climatic factors such as solar radiation, air temperature, wind speed and long-wave heat radiation. Temperature variations are often categorized into two components. A uniformly varying component, referring to the average temperature change, often induces expansion or contraction movements. The other linearly or nonlinearly distributed component, often causes bending deflections. Any restraints to these deformations can induce thermal forces. To calculate temperature-induced responses and evaluate the thermal effects on bridge behavior, the entire structural temperature distribution must be accurately known first.

Early studies of temperature effects on concrete bridges in the 1950s and 1960s generally focused on one-dimensional (1D) heat flow in the vertical direction using experimental data or empirical formulas (Zuk 1965). Analytical equations and numerical methods have also been proposed to calculate the temperature distribution of simple structures, including girder bridges, since the 1970s (Priestley 1972; Emerson 1973). These methods are basically 1D, can hardly capture the temperature variation and distribution of relatively complicated structures. Emanuel and Hulsey (1978) built two-dimensional (2D) models and investigated the effects of weather data on the sectional temperature distribution within concrete-steel composite bridges. Elbadry and Ghali (1983) proposed a 2D FE method to determine the time-dependent temperature variation of a concrete box-girder bridge by considering geometry, location, orientation, material, and meteorological conditions. Mirambell et al. (1990) determined the transverse temperature differences between the inside and the outside of concrete box bridges. Fu et al. (1990) developed a 2D analytical thermal model and conducted parametric analyses on steel-concrete composite bridges, and found that the ratio of the slab overhang length to the girder depth was the most influential factor on the temperature distribution.

For prestressed concrete (PC) bridges, several researchers examined the thermal effects including laboratory tests, field investigations and theoretical or numerical

analyses. Shushkewich (1998) used data from a PC segmental bridge in Hawaii to determine the critical positive and negative thermal gradients. The results were quite close to the design gradient specified by the AASHTO Segmental Guide Specifications (AASHTO, 1998). Roberts-Wollman et al. (2002) analyzed concrete temperature data of a segmental box-girder bridge in San Antonio over a 2.5 year time period, and compared the maximum recorded positive and negative thermal differentials to design recommendations. Li et al. (2004), after analyzing experimental data, proposed a vertical temperature gradient for deep PC box-girder sections. Lee (2010, 2012) conducted experimental and analytical studies on a PC BT-63 girder segment to determine the transverse and vertical temperature gradients. Hedegaard et al. (2013) measured thermal gradients through the section of the I-35W St. Anthony Falls Bridge, a posttensioned concrete box girder bridge in Minneapolis over the course of 3 years. The magnitudes and shapes of the measured thermal gradients were compared with various design gradients, and a fifth-order curve was found to best approximate the shape of the gradients.

The AASHTO LRFD specification (2012) has provisions for predicting longitudinal thermal expansion in bridges, which depends on the range of mean bridge temperature. The temperature range specified by AASHTO is based on two procedures (A and B). This method of predicting bridge temperature ranges and the resulting movements will be used for a PC bridge in Oklahoma, and the results will be compared with that from finite element structural analysis and filed measurement. AASHTO LRFD (2012) also provides the recommendations for load factors of uniform temperature (γ_{TU}) and thermal gradient (γ_{TG}) for different load combinations at different limit states. However, on the basis of temperature loading investigated in paper 1, the maximum daily positive gradients consistently occurred around 2 to 4PM, which implies a possible correlation between live loading around rush hour and maximum thermal gradient effects. If large live loading and thermal effects are correlated, the live load factor equal to zero for service limit states with the full design gradient might be un-conservative. Further statistical investigation is required to resolve these issues. With the increasing number of more complex and longer-span bridges being constructed in Oklahoma, where temperature ranges well in excess of 100°F may be observed over the course of a year,

a better understanding and more accurate consideration of thermal loading effects should be reflected in bridge evaluation and rating methodologies. Furthermore, in older bridges, due to deterioration of various bridge components, understanding the thermal loading becomes critical in condition evaluations and prioritizing bridges for repairs.

This research develop a method to incorporate the effects of self-straining thermal actions, where necessary, in reliability-based condition evaluation and capacity rating of bridges in Oklahoma.

2 Critically appraise current approaches to addressing thermal effects in highway bridges in literature

2.1 AASHTO design specifications

2.1.1 AASHTO Standard Specifications for Highway Bridges

The information regarding thermal effects in the AASHTO Standard Specifications for Highway Bridges (2002) is contained in Section 3.16, which states:

> *"Provision shall be made for stresses or movements resulting from variations in temperature. The rise and fall in temperature shall be fixed for the locality in which the structure is to be constructed and shall be computed from an assumed temperature at the time of erection. Due consideration shall be given to the lag between air temperature and the interior temperature of massive concrete members or structures."*

For metal structures, the range of bridge temperature should generally be taken as 0 ~ 120 °F under moderate climate and -30 ~ 120 °F for cold climate (AASHTO, 2002).

As indicated above, the standard specification provides a temperature range for moderate and cold climates to be used in design of metal structures, like steel bridges. The specification stipulates that provisions should be made for the stresses or movements generated by the temperature variations in the bridge.

2.1.2 AASHTO LRFD Bridge Design Specifications

More detailed information on thermal loading is provided in the AASHTO LRFD Bridge Design Specification (2014) than the AASHTO Standard Specifications. The LRFD Specifications indicate that the design thermal movement associated with a uniform temperature change can be calculated using either Procedures A or B, which are discussed in the following subsections.

2.2 AASHTO LRFD Design Thermal Movement Procedure A

Procedure A in the LRFD Specification is analogous to the approach recommended in the AASHTO Standard Specification. The temperature ranges in **Table 2-1** address moderate and cold climates, as in the Standard Specification. Section C3.12.2.1 of the commentary to the LRFD, defines the distinction between moderate and cold climates based on the number of freezing days per year. If the number of freezing days is less than 14, the climate is considered to be moderate. Freezing days are defined as days when the average temperature is less than 32 ºF.

Table 2-1. AASHTO LRFD Procedure A Temperature Ranges

Climate	Steel or Aluminum	Concrete	Wood
Moderate	0^o to 120^o F	10^o to 80^o F	10^o to 75^o F
Cold	-30^o to 120^o F	0^o to 80^o F	0^o to 120^o F

Using the AASHTO LRFD procedure the change in temperature is defined as the difference between a lower/upper bound temperature from the table and the temperature at which the bridge was erected. This temperature range is multiplied by the thermal coefficient of expansion of the material being designed and by the length of the member being designed.

2.3 AASHTO LRFD Design Thermal Movement Procedure B

Procedure B utilizes a design temperature range defined through a thermal contour map of the United States. Different maps are given for concrete decks on concrete beams and concrete decks on steel beams. The maps provide the maximum design bride temperature (TMaxDesign) and minimum design bridge temperature (TMinDesign). The contour maps for concrete girder bridges with concrete decks are shown in **Figure 2-1** and **Figure 2-2**. The contour maps for steel girder bridges with concrete decks are shown in **Figure 2-3** and **Figure 2-4**.

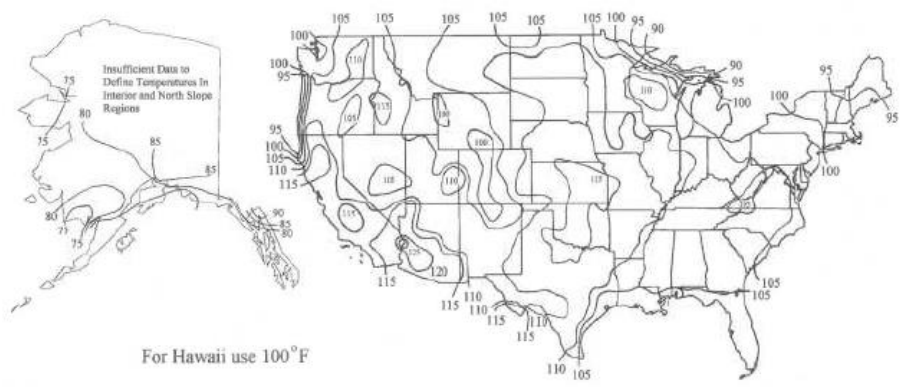

Figure 2-1. TMaxDesign for Concrete Girders with Concrete Decks (AASHTO 2014)

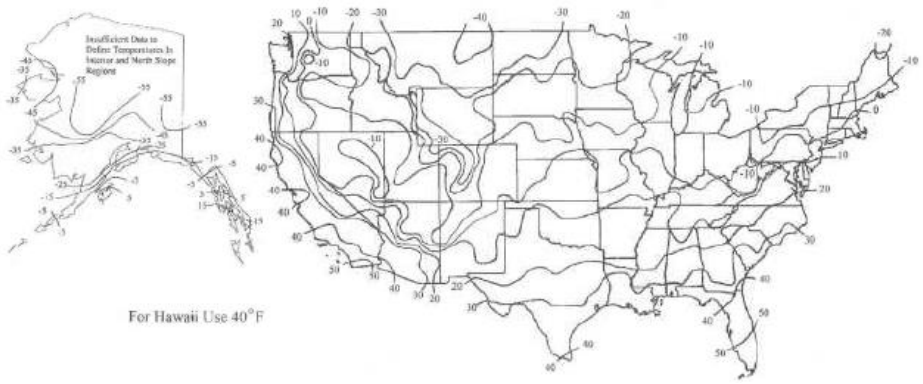

Figure 2-2. TMinDesign for Concrete Girders with Concrete Decks (AASHTO 2014)

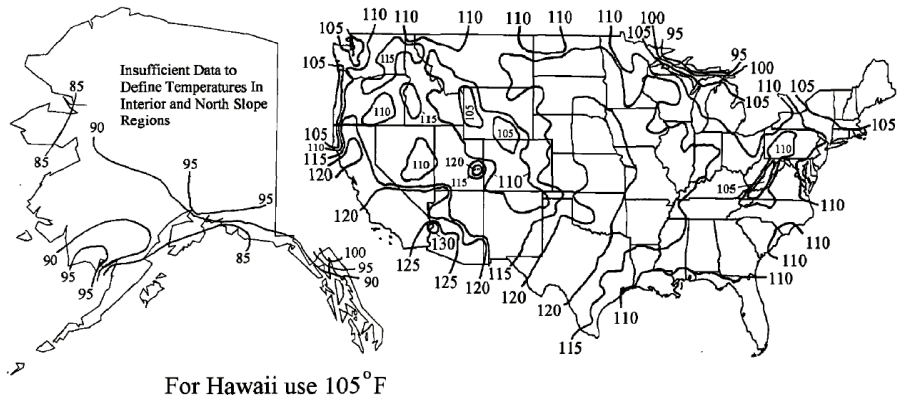

Figure 2-3. TMaxDesign for Steel Girders with Concrete Decks (AASHTO 2014)

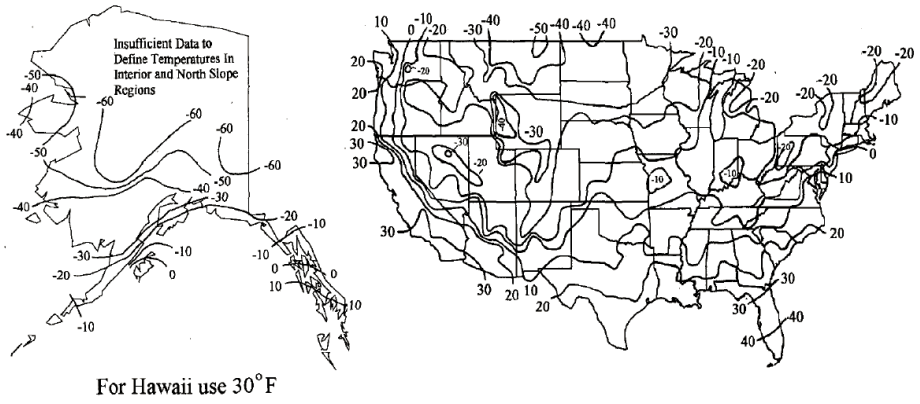

Figure 2-4. TMinDesign for Steel Girders with Concrete Decks (AASHTO 2014)

The expressions for the design movements for joints and bearings are based on the standard Equation 1-1. In the AASHTO LRFD Specification Procedure B, ΔT is defined based on the difference between TMaxDesign and TMinDesign.

$$\delta_t = \varepsilon_t L = \alpha(\Delta T) L \tag{1}$$

where α is the coefficient of thermal expansion of material, ΔT is a change in temperature, L is the length

2.4 AASHTO LRFD Design Temperature Gradient

The AASHTO LRFD Bridge Design Specification also contains a thermal gradient, which is shown in **Figure 2-5**. The gradient varies depending on whether the beams are concrete or steel. The dashed line represents the thermal gradient for steel bridges in the figure, dimension “A” for steel girders is 12 inches and “t” is the depth of the concrete deck, For concrete superstructures that are 16 inches or more in depth, dimension “A” is 12 inches, while the concrete sections shallower than 16 inches, dimension “A” is 4 inches less than the actual depth. Temperature “T3” may be taken as zero unless a site-specific study of temperatures is conducted. Temperatures “T1” and “T2” vary by location (zone 1-4), as shown in **Figure 2-6**.

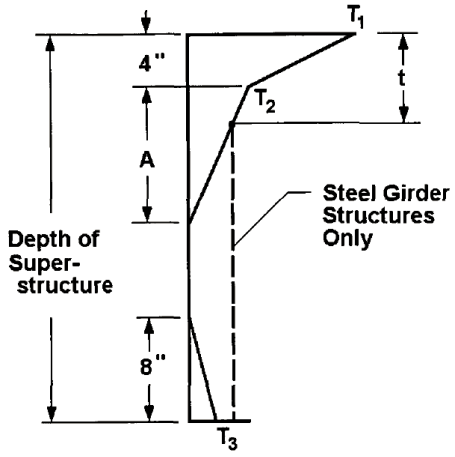

Figure 2-5. Positive Vertical Temperature Gradient in Superstructures (AASHTO 2014)

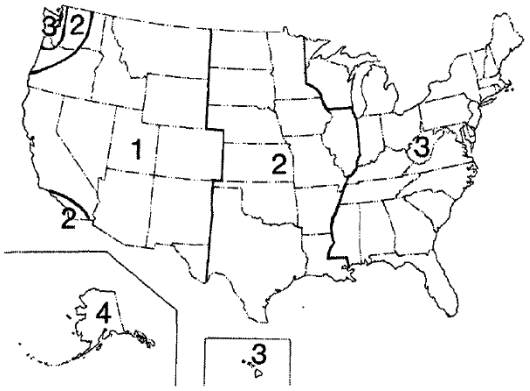

Zone	T_1 (°F)	T_2 (°F)
1	54	14
2	46	12
3	41	11
4	38	9

Figure 2-6. Solar Radiation Zones for the United States (AASHTO 2014)

The solar zones in **Figure 2-4** generally run north-south, and are reminiscent of time zones. The map apparently does not consider latitude to be of importance in determining the magnitude of the temperature gradient. It is unclear why solar radiation in the United States would vary by longitude and not latitude.

AASHTO Guide Specifications for Horizontally Curved Steel Girder Highway Bridges

The recommendations for consideration of thermal effects in the AASHTO Guide Specifications for Horizontally Curved Steel Girder Highway Bridges (2003) follow the recommendations of the AAHSTO Standard Specification, with the addition of temperature differential between the deck and girders, which states:

"Load effects in the superstructure shall be determined for uniform temperature changes as specified in AASHTO Article 3.16. A uniform temperature difference of 25 degrees Fahrenheit between the deck and the girders shall be considered when the width of the deck is less than one fifth of the longest span. The load effects due to the temperature differential shall be added to the effects due to the temperature changes specified in AASHTO 3.16."

Additional comments regarding orientation of bearing guides are contained in the commentary of the Guide Specification.

2.5 Conclusions and Recommendations

The thermal load, which provides foundation for calculating thermal stresses, is one of the key parameters that affect the service ability of bridges. The research of thermal load in bridge by theoretical model, numerical analysis, and field measurement is progressed remarkably, and design guidance about thermal loads is also provided in specifications for general form of bridges. However, it is far from sufficient. At least, the following aspects need to be further attempted.

(1) New concepts are employed in bridge design continuously. A lot of new bridges with complicated geometric configuration are constructed. At the same time, new materials

are invented for bridge structures. The heat properties such as emissivity and absorptivity of those new materials are different from general cases. For those bridges, the existing design specifications are useless. In addition, the global climate has much difference with that in several decades ago because of the development of industry and improvement of technology. So it is important to investigate thermal load in bridge with different schemes comprehensively.

(2) Due to the complexity of heat transfer and heat exchange, it is difficult to predict the thermal load for all the cases and codify the results to simple rules and guidelines that accommodate climatic, geographic, geometric, and material variations. Definition of critical thermal loads varying from region to region, bridge to bridge, and section to section becomes significant. In addition, the modern transportation system had been extended to the extremely cold area and extremely hot area, but the research of thermal load on bridge in those regions has attracted little attention.

(3) It is impossible that the temperature distribution in a bridge is described completely by limited data obtained by temperature sensors. So numerical models are powerful supplements. However, up to now, fine numerical models including all key components for simulating temperature distribution in large-scale bridges have not been developed. The intensity of solar radiation, the coupling effect of air temperature and wind speed, and the heat exchange between the surface and surrounding environment are not defined exactly. Moreover, the perfect transition from heat transfer analysis to thermal stresses analysis is not achieved.

(4) Current specifications provide engineers with a temperature gradient across the depth of the cross section to predict the vertical thermal behavior of bridges based on one-dimensional heat flow. But the specifications do not provide any guidance for transverse temperature gradients that cause additional lateral deformations in the girders especially prior to the placement of the bridge decks during construction. Investigation results already demonstrated that those transverse temperature differences exist in many bridges and the values are greater than those of vertical temperature differences sometimes.

3 Finite element modeling, calibration and temperature effect analysis of selected sample bridges

3.1 Bridge description

The researched bridge is located at the intersection of I-35 (under) and 19th Street in Cleveland County, Oklahoma (**Figure 3-1**). This is a simply supported prestress concrete bridge with two spans, each span has a length of 135 ft 3-5/8 in (41.24m), and the total length of this bridge is 270ft 7-1/4 in (82.48m), the total width and height of this bridge is 70ft 4-7/8 in (21.46m) and 6ft 10-7/8 in (2.1m), respectively. The structure includes a concrete deck supported on ten I-shaped prestressed concrete girders. The width and thickness of the bridge deck are270ft 7-1/4 in (82.48m) and 7-7/8 in (0.2m) respectively, while the height of the girders is 6ft(1.83m). There are 34 tendons in the bottom slab and 4 tendons in the top slab in each the PC girder, the diameter of all the tendons is 0.6in (0.015m). Two end diaphragms with the thickness of 12in (0.3m) and two middle diaphragms with the thickness of 10in (0.25m) are installed to enhance the transverse stiffness of the bridge.

Figure 3-1. 19th Street/I-35 Bridge

3.2 Finite element thermal analysis

To predict nonlinear temperature distributions in the selected bridge, a two-dimensional (2D) finite element heat transfer analysis is performed using measured environmental conditions: solar radiation, ambient air temperature, and wind speed. The solar radiation

is applied to the top, vertical and inclined surfaces of the girder as a heat source according to the position of the sun, the location of the bridge, the geometry of the girder, and the measured solar radiation on the horizontal surface. The ambient air temperature and wind speed are used to account for heat convection boundary conditions in the heat transfer analysis. The girder temperatures obtained from the heat transfer analysis are then compared with those measured in the field load test.

3.2.1 Finite element model for thermal analysis

With an assumption of a constant temperature variation in the longitudinal direction of the girder, the cross section of I35-19th Bridge was modeled using a 2D element, PLANE55, in ANSYS (2014). A total of 5982 elements and 5385 nodes were used for the cross-section as shown in **Figure 3-2**. With the finite element model determined, a 2D heat transfer analysis was performed which consisted of four heat transfer phenomena: heat conduction in the concrete, heat convection between the surroundings and the concrete surface, heat irradiation from the sun, and heat radiation to the surroundings. Reflected radiation between the surfaces of the girder was ignored. The initial reference temperature was assumed to be constant over the cross-section based on an average of all the measured temperatures at the start time of the analysis, 12 a.m. For example, on July 22, the constant initial temperature was found to be 25°C (77°F), as shown in **Figure *3-3***.

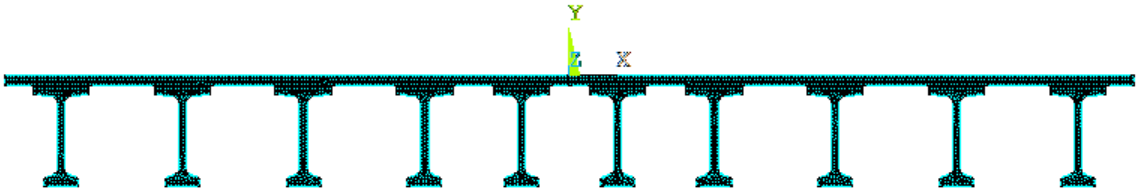

Figure 3-2. Two-dimensional ANSYS Finite Element Model

3.2.2 FE thermal analysis results

July 22, 2014 is arbitrarily chosen to demonstrate the comparisons between measured and predicted results for the purposes of validation. In the interest of clarity and practicality, select results are presented. The values presented are representative of the degree of comparison observed on different days as well as at various regions throughout the bridge. The environmental data on July 22, 2014 including ambient temperature (**Figure 3-3**), wind speed and solar radiation on surfaces (**Figure 3-4**) were input into both the two-dimensional models.

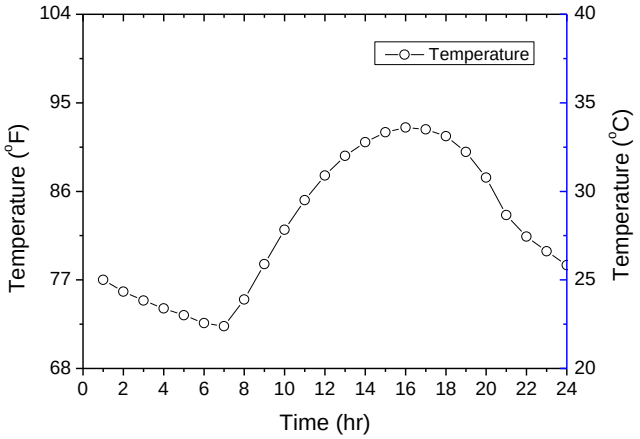

Figure 3-3. Hourly Ambient Temperature on July. 22, 2014

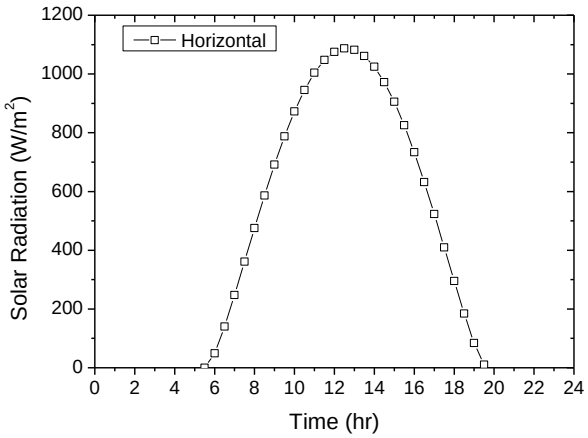

(a) Solar radiation at horizontal surface

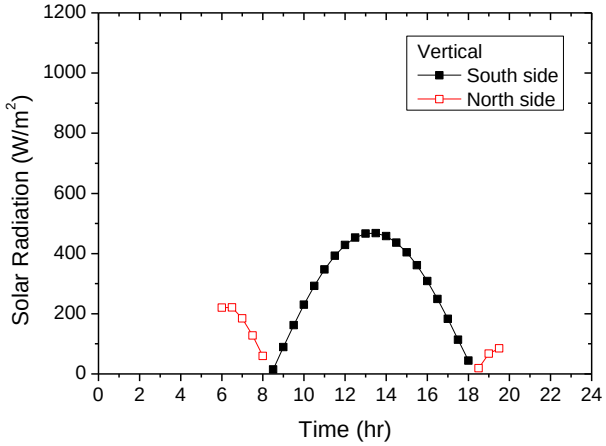

(b) Solar radiation at vertical surface

Figure 3-4. Hourly Solar Radiation on July. 22, 2014

3.3 Temperature History

Temperature histories obtained from the heat transfer analysis are obtained and compared with the measurements along the vertical and lateral directions of the cross section. Both outer girders (e.g. girder 1) and inner girders (e.g. girders 3, 5) are included, as shown in **Figure 3-5**. And **Figure 3-6** shows the temperature histories on different positons (slab, top and bottom flanges, and web) for girder 1 on July 22, 2014, respectively. The results showed that the highest temperature in the vertical temperature distribution was on the top surface and the lowest temperature in the

bottom flange, and the highest temperature occurred at about 17pm. Also, the outer and inner girders have the same trends of temperature histories.

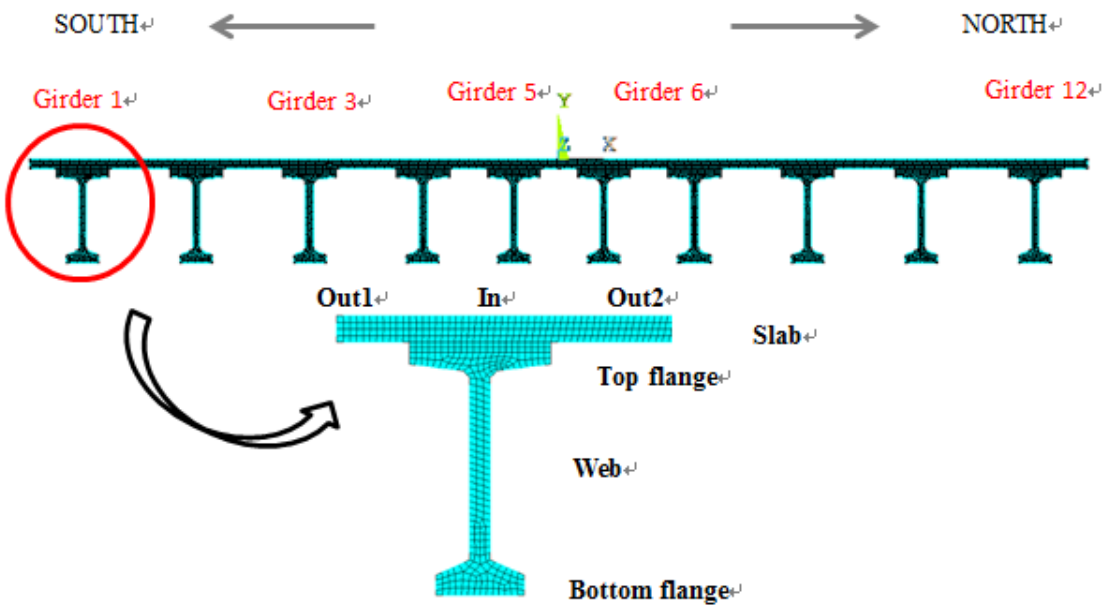

Figure 3-5. Cross Section

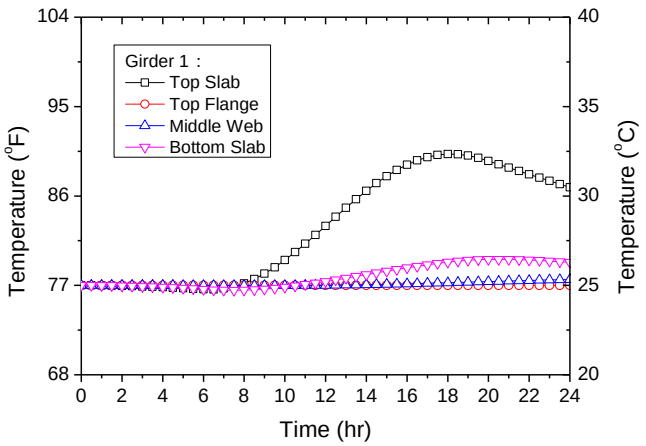

Figure 3-6. Temperature histories of girder 1 on July. 22, 2014

In addition to vertical temperature variations, **Figure 3-7** shows the predicted transverse temperature variations in the slab on July 22, 2014. The highest temperature in the top

flange was on the south end of the top flange (Flange-Out1) while the lowest temperature was in the middle of the top flange (Flange-In). The slab, web and bottom flange have the similar trends, the south-facing surface (Out1) exhibited the highest value, and the north-facing middle (In) of components showed the lowest value. Because the south-facing surfaces are directly subjected to solar radiation, while the temperature of middle surfaces is translated from the outer surface.

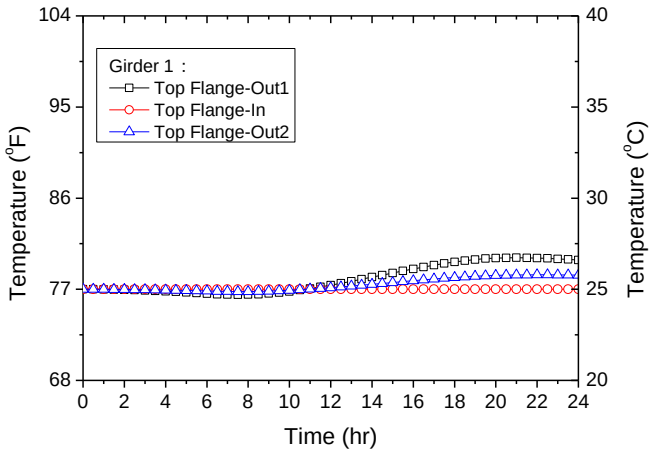

Figure 3-7. Temperature histories in top flange on July. 22, 2014

3.4 Sectional Temperature Distribution

The temperature distributions across the width of the bridge were calculated from the two-dimensional ANSYS model and are also compared with field measurements on the chosen day. Only the distributions at 17 pm are shown in **Figure 3-8**. At 17 pm, it can be seen that the sunlit part of the exterior girder is much warmer than the shaded portions. The higher temperatures are also apparent at the top of the slab on both sides of the bridge since the top of the slab would be exposed to direct sunlight.

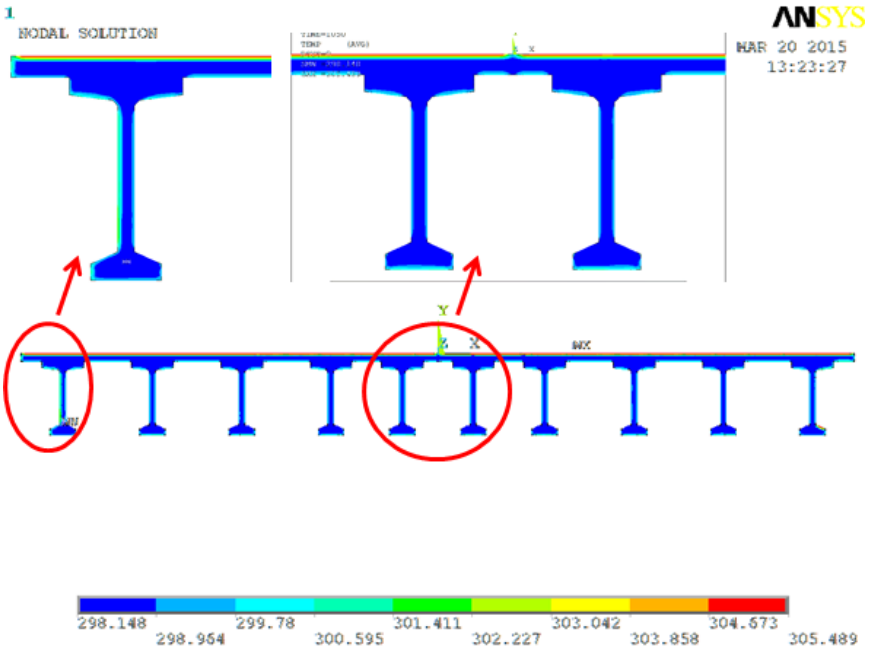

Figure 3-8. Sectional temperature distribution at 17 PM, 07/22/2014 (Unit: oK)

In addition, **Figure 3-9** shows the predicted maximum vertical temperature distributions along the depth of the girder 1 section for July 22, 2014. The difference of temperature on the slab between that on the web is 13 °F, while the difference of temperature on the web between that on the bottom flange is 5 °F. The temperature decreases almost linearly from the top of slab to the web rapidly along the depth of the cross-section, also with the same trend from the bottom of flange to the web.

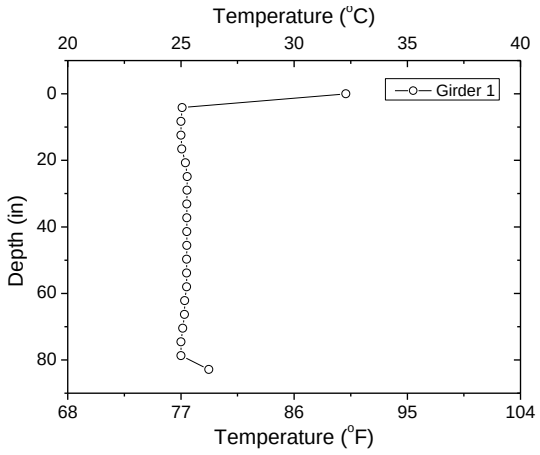

Figure 3-9. Vertical temperature distributions along the depth of Girder1 at 17 PM, 07/22/2014

In addition to vertical temperature distributions, **Figure 3-10Figure 5-9** to **Figure 3-11** show the predicted transverse temperature distributions across the top flange, the middle of the web of girder1, respectively. Across the top flange, a maximum difference of 2.0°F on July 22 occurred at the south end of the top flange. The middle of the web showed a maximum difference of 5°F on the south vertical surface of the web flange.

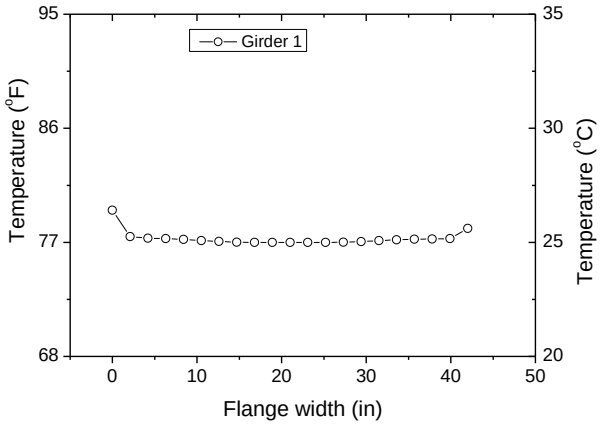

Figure 3-10. Transverse temperature distributions across the top flange of Girder 1 at 17 PM, 07/22/2014

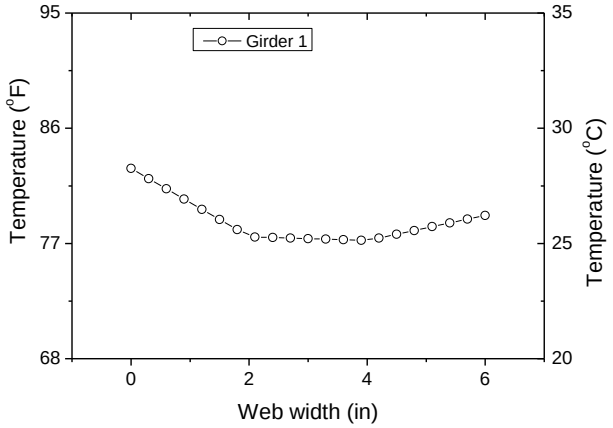

Figure 3-11. Transverse temperature distributions across the middle of the web of Girder 1 at 17 PM, 07/22/2014

3.4.1 Finite element model for structural analysis

The I35-19th Bridge was modeled using 3D solid elements- SOLID45, 3D elements-LINK180, and spring elements-COMBIN14in ANSYS (2014). The required compressive strength of concrete for slab, girders and diaphragm is 10,000psi at 28days. The type of tendons required in the P.C girders is low relation 7- wire strand with normal diameter of 0.6 inches and ultimate tensile strength of 270ksi. All the materials in this simulation are assumed in elastic stage. The researched bridge is simply supported on the abutment and piers. Considering different restriction degree of bearings which supporting the P. C. girders, spring elements are used to simulate the bearings with different stiffness. The 3-D FE model of I35-19th Bridge was shown in **Figure 3-12**. To understand the structural behavior of researched bridge, dead load (self-weight)-Load case 1, live load (a uniformly pressure of 100lb/ft2) -Load case 2 and thermal load (non-uniform temperature field: top slab 46°F, bottom flange 12°F) -Load case 3 are applied respectively.

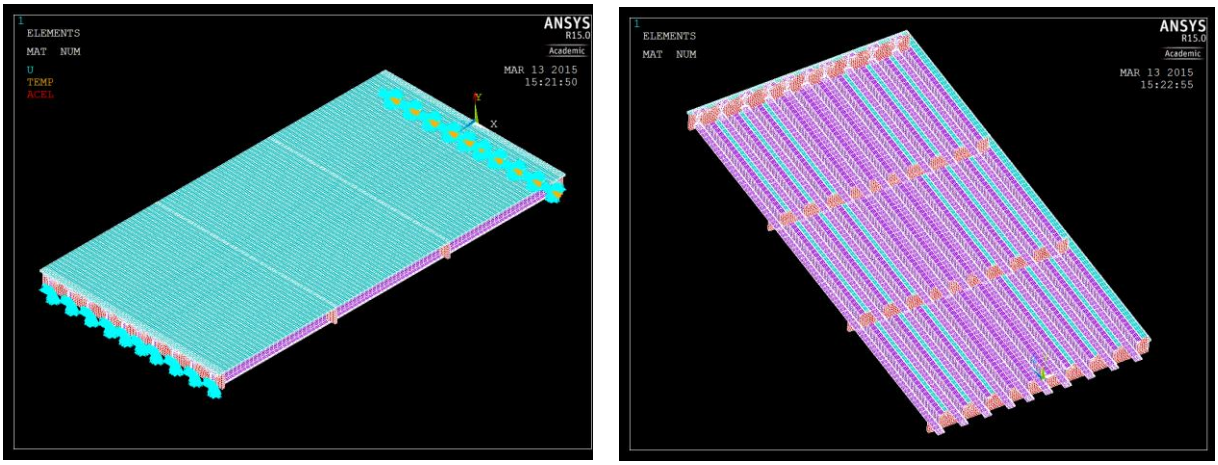

(a) Whole structure in top view (b) Whole structure in bottom view

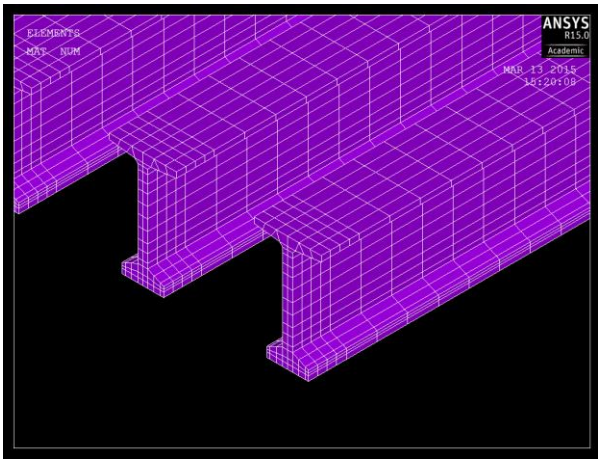

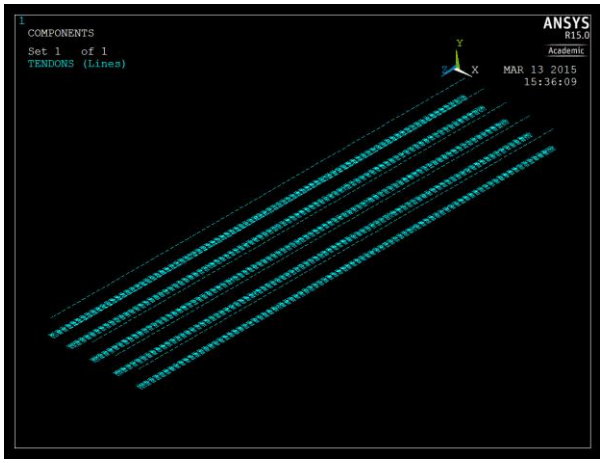

(c) P.C. girders (d) Tendons

Figure 3-12. Three-dimensional ANSYS Finite Element Model

3.4.2 FE thermal analysis results

Due to the limited space, only the displacement contour figures under load case 3 are shown in **Figure 3-13** in transversal, vertical and longitude directions respectively. The maximum value of transversal, vertical and longitude displacement under all three load cases are list and compared to the calculated ones from Matlab model in **Table 4-1**.

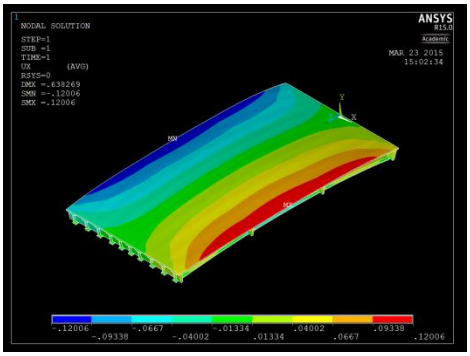

(a) transversal

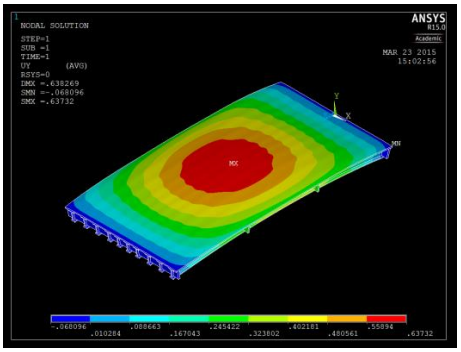

(b) vertical

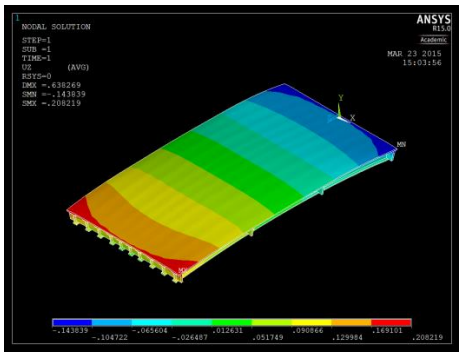

(c) longitude

Figure 3-13. Displacements under load case 3 from ANSYS

4 Development of simplified modeled using MatLab for time-efficient thermal stress analysis

A simplified model derived from fundamental energy principles which include shearing and in-plane translations as well as normal motions and possibly nonlinear effects has been developed. In developing the MatLab models, a key objective is to develop models that capture salient features of the bridge behavior under thermal loading while remaining sufficiently simple to permit fast computational solutions.

And this simplified MatLab model was calibrated by the finite element model of the select sample bridge I35-19th Bridge. The concrete slab, PC girders were simulated as plate elements. The interaction between the bridge and abutments are included through proper modeling of the boundary conditions using spring elements with proper stiffness. The geometrical dimensions, material properties, boundary conditions and load cases were chosen the same as the 3D finite element models in **Figure 3-2**. The displacement contour figures under load case 3 calculated using Matlab model are shown in **Figure 4-1** in transversal, vertical and longitude directions respectively.

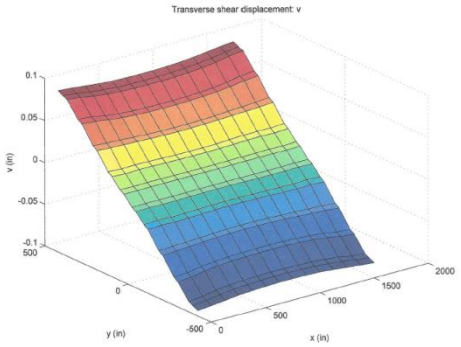

(a) transversal

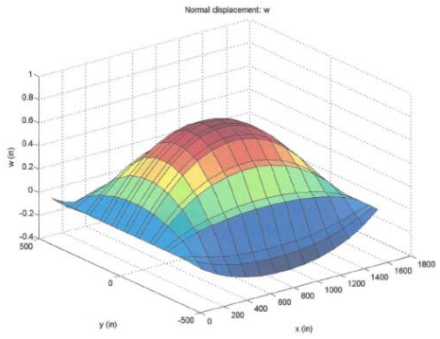

(b) vertical

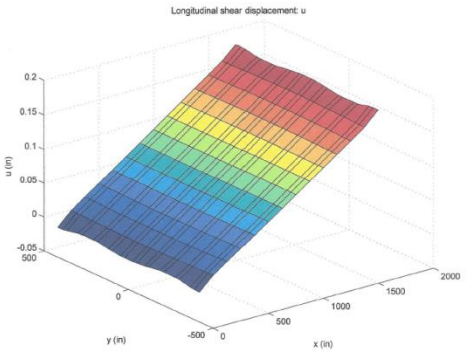

(c) longitude

Figure 4-1. Displacements under load case 3 from Matlab

The displacement results from MATLAB model are compared with that from FE model using ANSYS, as shown in **Table 4-1**. It can be found that these two models agree well with the defection shape and value in both vertical direction and transversal direction, these two models agree well with the deformation shape in longitudinal direction, but there is some difference in the value. it maybe MATLAB model has more longitudinal constrain, as the MATLAB model simulate the girder as plate element, the whole cross section in the end is restricted in longitudinal direction. But only the bottom of flange in ANSYS model is restricted, the cross-section at end can rotate in ANSYS model. In all, the simplified MATLAB models were verified by the ANSYS model and will be used to perform the probabilistic study and uncertainty analysis described in Task 5.

Table 4-1. Displacements comparison from ANSYS and Matlab

Load case	Calculation model	Transversal displacement (in)	Vertical displacement (in)	Longitude displacement (in)
1	ANSYS	0.012	1.56	0.31
	MATLAB	0.01	1.5	0.3
2	ANSYS	0.005	0.58	0.12
	MATLAB	0.006	0.6	0.12
3	ANSYS	0.12	-0.64	0.21
	MATLAB	0.1	-0.6	0.18

5 Analyze Oklahoma Mesonet database

The Oklahoma Mesonet is a world-class network of environmental monitoring stations which consists of 120 automated stations covering Oklahoma. There is at least one Mesonet station in each of the Oklahoma's 77 counties. At each site, the temperature, precipitation, humidity, wind speed, etc. are concurrently measured by a set of instruments located on or near a 10-meter-tall tower. The measurements are packaged into "observations" every 5 minutes and the observations are transmitted to a central facility every 5 minutes, 24 hours per day year-round. The Oklahoma Climatological Survey (OCS) at OU receives the observations, verifies the quality of the data and provides the data to Mesonet customers. Based on the relationships between the environmental conditions and the largest vertical and transverse temperature differentials, the Oklahoma Mesonet, which contain the 20-year (from 1994 to 2014) daily solar radiation, climatic values, wind speed, were evaluated for extremes in environmental conditions.

5.1 Air Temperature

For expected daily extremes in air temperature, the Oklahoma Mesonet data pertaining to the record daily maximum and minimum temperatures were investigated. The record daily maximum and minimum temperatures were obtained from the entire record period of 1994 to 2014. **Figure 5-1** shows the record daily maximum, minimum, average temperatures extracted from the Mesonet data for the Norman station, from 1994 to 2014. **Figure 5-2** shows the extreme temperature from Jan. to Dec. during the past 20years.

For Aug 1 (2012), the record daily maximum temperature was obtained, which was 43.3°C (109.9°F). Also, the record daily minimum temperature was found as -18.2°C (-0.8°F), on Feb.4 (1996). The record daily maximum temperature difference (maximum –

minimum temperature at the same day) was 30.9 °C (87.6°F), the occurred on Feb.4 (1996), the same day as the record daily minimum temperature. The details of daily maximum, minimum, average temperature and temperature difference of year 2012 presented in **Figure 5-3** as an example.

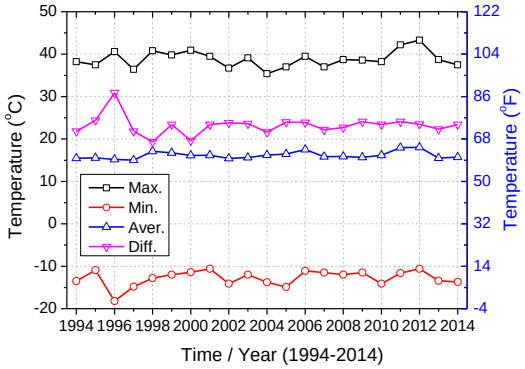

Figure 5-1. Yearly extreme daily air temperatures

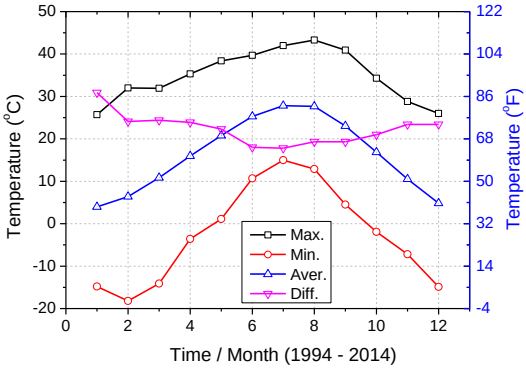

Figure 5-2. Monthly extreme daily air temperatures

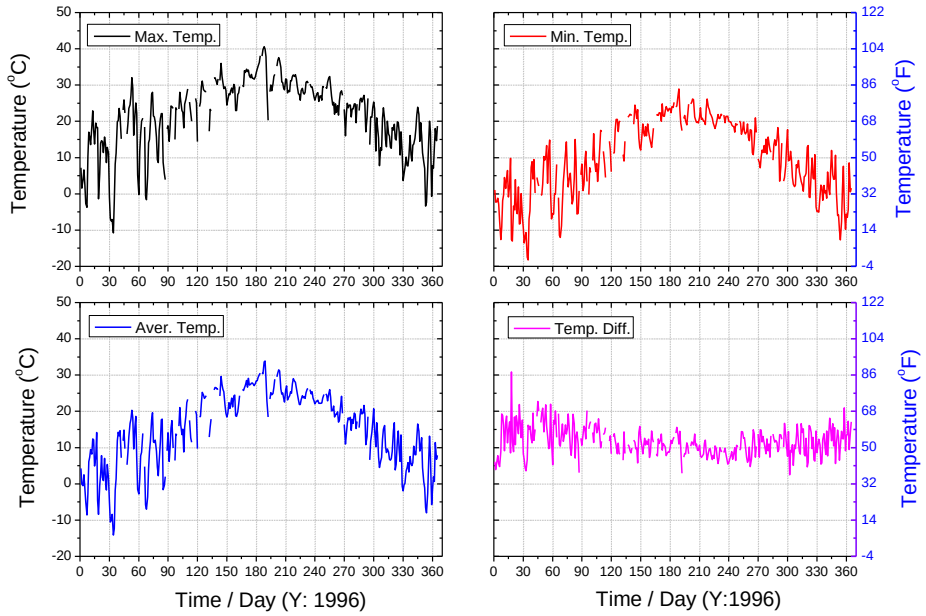

Figure 5-3. Extreme daily air temperatures for 2012

The air temperature affects the variation in the temperature distributions of bridge girders. In general, hourly ambient air temperatures are available from measurement. If they are not available, a sinusoidal daily cycle between the minimum and maximum temperatures, Tmin and Tmax, can be used to interpolate them.

$$T_{air}(t) = \frac{(T_{\max} + T_{\min})}{2} + \frac{(T_{\max} - T_{\min})}{2} \sin\left[\frac{\pi(t-9)}{12}\right] \quad (2)$$

in which Tair(t) = the air temperature as a function of time t, Tmax = the daily maximum air temperature, and Tmin = the daily minimum air temperature.

Variations in air temperature predicted by the equation were compared with those measured on Aug. 1, 2012 and Dec. 8, 2005, as shown in **Figure 5-4**. These two days represent typical summer and winter days respectively. According to **Figure 5-4**, the equation4-1 provides good correlations with the measurements on these two days.

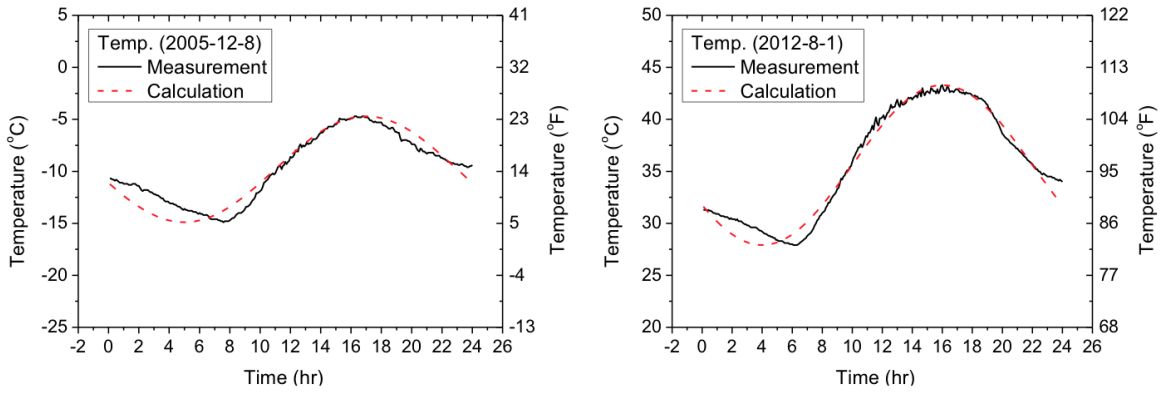

Figure 5-4. Comparison of the air temperature measured every five minutes and the predicted hourly air temperature

5.2 Wind speed

For another environmental factor of wind speed, the record maximum and average daily wind speed were obtained during the entire record period of 1994 to 2014 from Oklahoma Mesonet data. The daily average wind speed calculated by integrating the measurement data using the trapezoidal numerical method and dividing the integration by the total measuring time was within 1 m/sec (2.2 mph) with no specific seasonal variations. **Figure 5-5** shows the record daily maximum, average wind speed, from 1994 to 2014. **Figure 5-6** shows the record daily maximum, average wind speed from Jan. to Dec. during the past 20years. The maximum wind speed was recorded as 21.9 m/sec, on May 31-2012, as shown in **Figure 5-7**. The recorded average wind speed from the measured wind speed data was less than 5 m/sec (11.2 mph) on the days when the large vertical and/or transverse temperature differentials were recorded. Therefore, in this study, the effect of wind speed on temperature variations in bridge girders was disregarded.

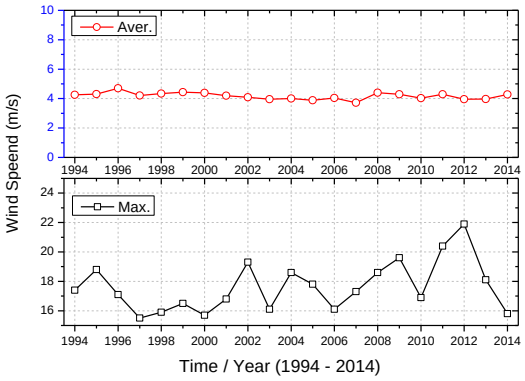

Figure 5-5. Max. and Ave. daily wind speed of each year

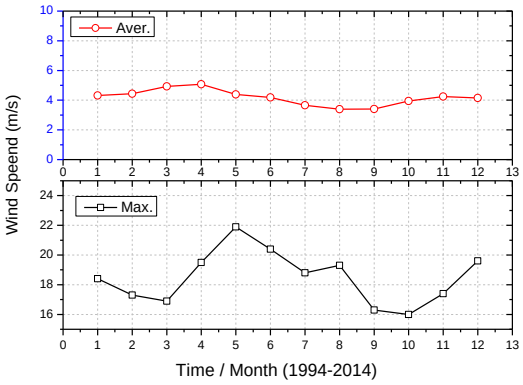

Figure 5-6. Max. and Ave. daily wind speed of each month

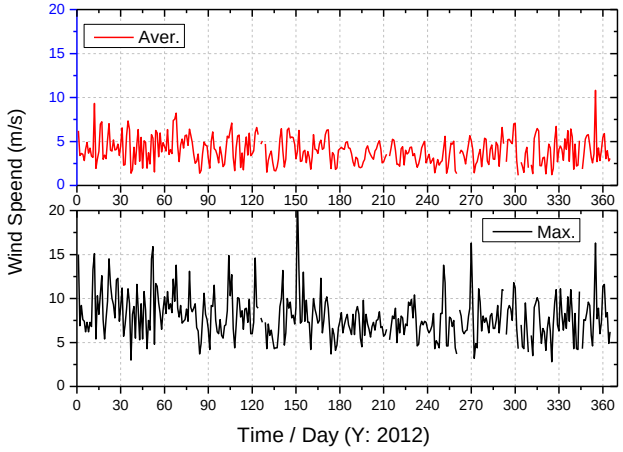

Figure 5-7. Maximum and average daily wind speed for 2012

5.3 Solar radiation

The Mesonet data also provide solar radiation at every 5 minutes from 1994 to 2014. The daily maximum and total solar radiation were obtained from each month and each year, as shown in **Figure 5-8** and **Figure 5-9** respectively. The total average daily solar radiation calculated from the measurements ranged from 28 to 32 MJ/m2 in the summer and from 14 to 18 MJ/m2 in the winter under clear sky conditions. In particular, on July 23,2000, the maximum daily solar radiation was 1362 w/m2, as shown in **Figure 5-10**.

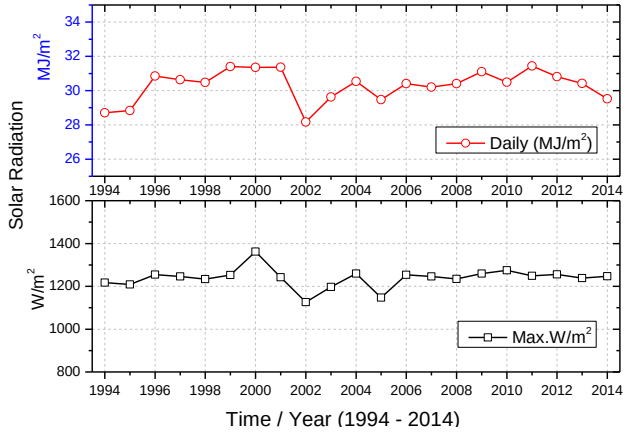

Figure 5-8. Max. and total daily solar radiation of each year

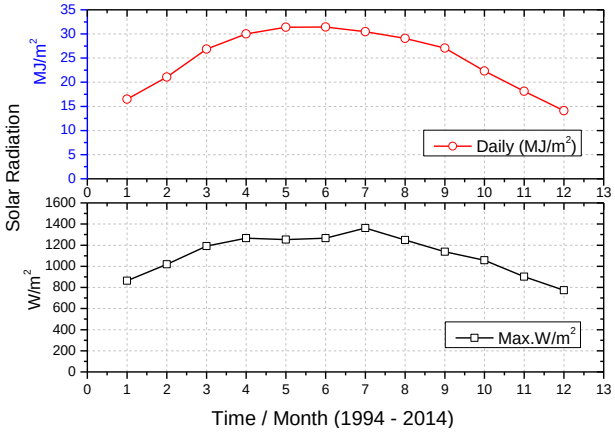

Figure 5-9. Max. and total daily solar radiation of each month

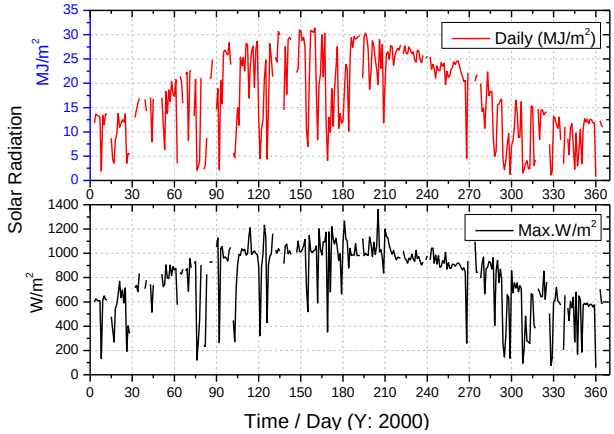

Figure 5-10. Maximum and total daily solar radiation for 2000

To evaluate the effectiveness of the equations of proposed solar radiation model on the variation in daily solar radiation over the length of a day, this study compared the predicted solar radiation with the measurements on a horizontal surface for Aug. 1, 2012 and Jan. 18, 1996. **Figure 5-11** shows the solar radiation on a horizontal surface measured every five minutes and the predicted hourly solar radiation using the equations of solar radiation model. The equations provide good agreement with the measurements. Thus, these equations can be used for the prediction of variations in solar radiation incident on the horizontal surface of PC bridge girders.

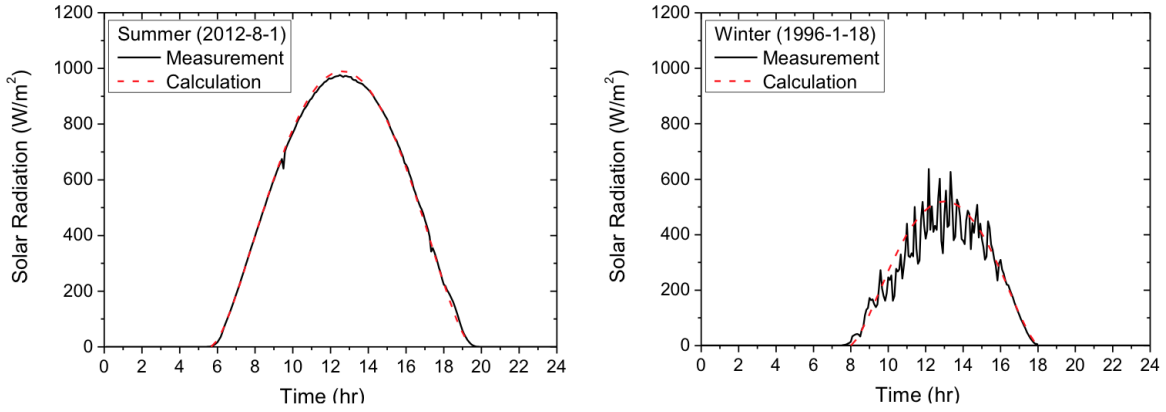

Figure 5-11. Comparison of the solar radiation measured on a horizontal surface and the predicted hourly solar radiation

6 Develop statistical descriptions of thermal stresses in bridges using simplified MatLab models

A probabilistic analysis is performed using the approximate bridge models to obtain a probabilistic description of the thermal stresses. This probabilistic model reflect the uncertainties in daily and seasonal temperature profiles which developed in Task 4 as well as the uncertainties in structural and material properties of the bridge that affect its behavior under thermal loading, including material thermal conductivity, continuity over supports, and other geometry and constraint characteristics. Latin hypercube sampling and Monte Carlo Simulation are used to propagate the uncertainties in strength, loadings and thermal effects through the simplified bridge model.

6.1 Probabilistic model of temperature profiles

In order to obtain statistical modeling of the temperature load model, which should reflect the likely value (mean or median) and uncertainty of the extreme temperature range experienced by a bridge in 75 years of service life, finite element thermal analysis were conducted on the sample bridge at extreme temperature conditions (Maximum solar radiation, Maximum temperature difference) from 1994 to 2014 based on the Oklahoma Mesonet database.

On the basis of FE simulation results, the temperature profile agrees well with the recommended one by AASHTO specification for positive temperature distributions. Therefore, we adopt temperature profile recommended by AASHTO specification, and use statistical modeling of the temperatures T1, T2 and T3 from simulation results, as shown in **Table 6-1**. **Figure 6-1** shows the PDF and CDF of T1 and the fitted normal distribution of T1. After the statistical modeling of the annual maximum temperatures T1, T2 and T3 was determined, the distribution function of the temperature data (T1, T2 and T3) are extrapolated to a full lifetime of 75 years based on extreme value theory, as shown in **Figure 6-2** and **Table 6-1**. Local bridge temperatures vary widely with time through the bridge cross section, but the average temperature of the bridge cross

section, T_{eff}, controls bridge movements, the probability distributions and estimate parameters of maximum and minimum T_{eff}, are also listed in **Table 6-1**.

Table 6-1. Summary of Parameter Estimates (°C)

Parameter	**Domain of Attraction**	***μ***	***σ***	**The shape *ξ***	**Return Period**			**AASHTO**
					50	**75**	**100**	
T_{eff} for Maxima	GEV	40.55	1.40	-0.14	46.02	**46.60**	47.00	46.11 (115°F)
T_{eff} for Minima	Gumbel	-2.21	0.97	N/A	-3.75	**-3.83**	-3.88	-6.67 (20°F)
T_1	Normal	17.98	1.3	N/A	20.65	**20.86**	21.00	25.56 (46°F)
T_2	Normal	6.58	1.17	N/A	8.98	**9.17**	9.30	6.67 (12°F)
T_3	Normal	2.13	1.23	N/A	4.65	**4.86**	5.00	2.78 (5°F)
D_1	Normal	-6.35	1.75	N/A	-9.94	**-10.23**	-10.42	-7.67 (-15.3°F)
D_3	Normal	-9.26	1.96	N/A	-13.28	**-13.60**	-13.82	-0.83 (-1.7°F)

Note: for Gumbel distribution, the location μ; the scale σ; for Normal distribution, The mean *μ;* The standard deviation *σ*

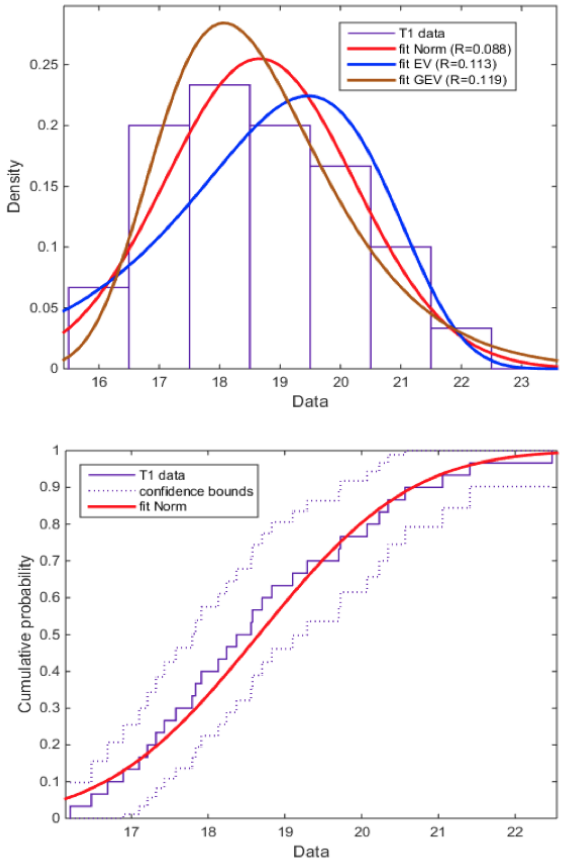

Figure 6-1. PDF and CDF of T1 and fitted normal distribution of T1

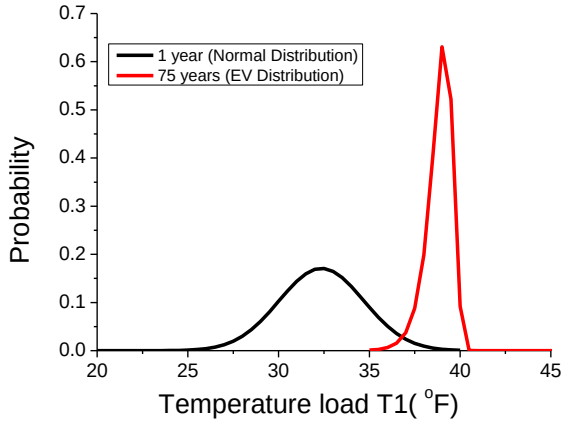

Figure 6-2. The distribution function of T1 extrapolated to a full lifetime of 75 years

Probabilistic model of temperature induced stress

The Monte Carlo Simulation (MCS) is used to simulate a bridge subjected to randomly generated loads and possessing uncertain resistance to obtain randomly generated bridge response (RGOVs), such as: (1) compressive stress at the top fiber at the mid-span; and (2) tensile stress at the bottom fiber at the mid-span. LHS method were adopted using software MATLAB to generate a set of temperature gradient (T1, T2 and T3; D1, D3), and corresponding uniform change temperature ($T_{eff\text{-}P}$ and $T_{eff\text{-}N}$). The compressive stress at the top fiber and the tensile stress at the bottom fiber for the mid-span section are the randomly generated bridge response that we are most concerned, both internal and external girder under simply support condition (SSC) and fixed end condition (FEC) are included. The distribution parameters of the temperature load response (stress) are obtained using MCS and statistical analysis and summarized in **Table 6-1**. To be consistent with the basis of the live load response used in calibrating the AASHTO LRFD Bridge Design Specifications, the statistical modeling of the temperature load response should reflect the likely value (μ) and uncertainty range (σ) experienced by a bridge in 75 years of service life. According to the extreme value theory, the asymptotic distribution of the largest value of compressive (or tensile) stress (normal distribution) is of the double exponential form (Type I), the parameters at return period of 75 years are also listed in **Table 7-1** and **Table 7-2**.

7 Develop a set of guidelines that are specific to Oklahoma climatology for consideration, where necessary, of temperature effects in bridge evaluation and capacity rating.

7.1 Reliability Analysis of AASHTO LRFD Limit State

Development of reliability-based bridge design load combinations with partial safety factors provides a consistent level of design safety. The proposed load combinations consider prestressing force, dead load (DL), traffic live load (LL), vehicular impact load

(IM) and thermal load (TG, TU). Distribution types and statistics for loads and resistances are determined based on published literature (Nowak 1995, 2003), and for thermal load based on MCS results in **Table 7-1** and **Table 7-2**.

Table 7-1. Summary of Parameter Estimate for stresses at the top fiber (MPa)

Load	Boundary Condition	Girder	Domain of Attraction	The Mean μ	The Standard deviation σ	Domain of Attraction (75 year)	The Mean μ (75 year)	The Standard deviation σ (75 year)
Positive temperature gradient (TG+)	Simply support (SSC)	G 1	Normal	-6.081	0.359	Gumbel	-6.962	0.157
Positive temperature gradient (TG+)	Simply support (SSC)	G 5	Normal	-6.134	0.358	Gumbel	-7.013	0.156
Positive temperature gradient (TG+)	Fixed end (FEC)	G 1	Normal	-8.99	0.54	Gumbel	-10.316	0.236
Positive temperature gradient (TG+)	Fixed end (FEC)	G 5	Normal	-9.17	0.556	Gumbel	-10.535	0.243
Positive uniform temperature (TU+)	Fixed end (FEC)	G 1	Normal	-3.426	0.683	Gumbel	-5.103	0.298
Positive uniform temperature (TU+)	Fixed end (FEC)	G 5	Normal	-3.789	0.57	Gumbel	-5.189	0.249

Table 7-2. Summary of Parameter Estimate for stresses at the bottom fiber (MPa)

Load	Boundary Condition	Girder	Domain of Attraction	The Mean μ	The Standard deviation σ	Domain of Attraction (75 year)	The Mean μ (75 year)	The Standard deviation σ (75 year)
Negative temperature gradient (TG-)	Simply support (SSC)	G 1	Normal	3.227	0.484	Gumbel	4.415	0.211
Negative temperature gradient (TG-)	Simply support (SSC)	G 5	Normal	3.79	0.597	Gumbel	5.256	0.261
Negative temperature gradient (TG-)	Fixed end (FEC)	G 1	Normal	4.003	0.598	Gumbel	5.471	0.261
Negative temperature gradient (TG-)	Fixed end (FEC)	G 5	Normal	4.511	0.711	Gumbel	6.257	0.310
Negative uniform temperature (TU-)	Fixed end (FEC)	G 1	Normal	5.037	0.755	Gumbel	6.891	0.330
Negative uniform temperature (TU-)	Fixed end (FEC)	G 5	Normal	5.691	0.729	Gumbel	7.481	0.318

The Rackwitz-Fiessler procedure producing an accurate result when basic statistics and distribution types of all related variables are provided, was adopted to compute reliability indices. Reliability analyses of AASHTO LRFD limit states (Service I, Service III and Strength I) are performed to determine whether additional thermal load reduce structure safety. A reliability analysis determines the safety level of a structure in terms of a

reliability index (β) and is computed here under two loading cases: (1) a bridge without thermal load; and (2) a bridge with thermal load, for two support conditions: (1) SSC; (2) FEC. Reliability indices (β) are computed for AASHTO limit states and presented in **Figure 7-1**, Both thermal load and boundary condition have significantly influences on β, the computed reliability indices represent very low probabilities of failures, and may result in a significant overdesign. Therefore, the load factors for thermal load should be re-computed to obtain a constant reliability index and to be consistent with the current AASHTO LRFD.

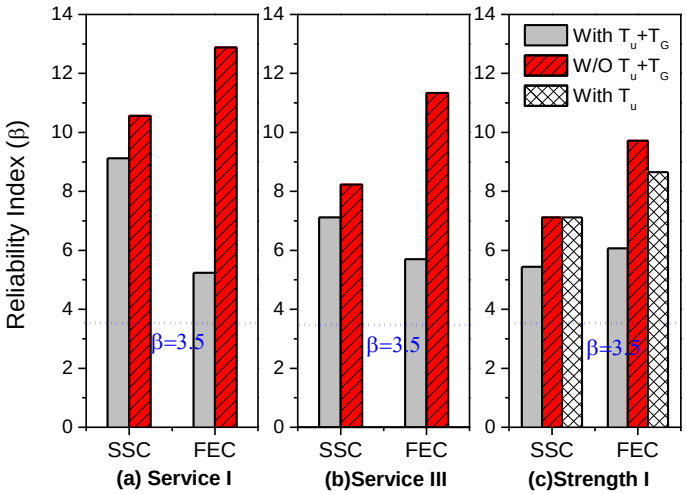

Figure 7-1. Limit State Reliability Indices

Reliability analyses were performed to determine the partial safety factors achieving target reliability index (β_T = 3.5) for AASHTO load combinations for Strength I limit state, using calibration procedure (Nowak, 1995). A resistance factor, φ_R, equal to 1.0 recommended by AASHTO LRFD for PC girders subjected to bending moment is applied to investigate γ_T.

For comparison purposes, boundary conditions are also considered. As for a simply supported bridge, if the temperature distribution is uniform or linear over the depth of the superstructure, the induced thermal stress or force are negligible. Even in a bridge

originally designed as a statically determinate structure with expansion joints can, over the years, become a statically indeterminate structure due to closing of the expansion joints at abutments and within the deck, additional thermal stresses may be induced due to axial or flexural restraints at supports. Since the restraint degree is difficult to estimate, fixed end supports were assumed in this statically indeterminate structure.

Based on the simple support condition, a reliability analysis was performed on AASHTO-PCI standard girder with BT-72 section (**Figure 7-2**) to get the nominal flexural strength (MRT) satisfying the target reliability index ($\beta_T = 3.5$). The TU and TG do not induce thermal force (MTU and MTG) in such statically determinate structure, only dead and live load are considered. To be consistent with AASHTO LRFD, load factors for DL, and LL+ IM are taken from Strength I limit state. The maximum span for BT-72 section is limited to 40m (130 ft) (PCI, 2003), therefore, the simply supported girders with two different spans (30m and 40m) were selected. The target nominal resistant moments (MRT), the design resistant moments (MRD) calculated based on the design parameters including the concrete strength (f'_C) and prestressing tendons (numbers Nps and positions D_{ps}) for simply supported girders with span of 30m and 40m are listed in **Table 7-3**. The ratio of MRD to MRT is 1.01, and β is reanalyzed to be 3.56 and 3.63 with the design parameters of the girder with span of 30m and 40m, slightly larger the target reliability index 3.5.

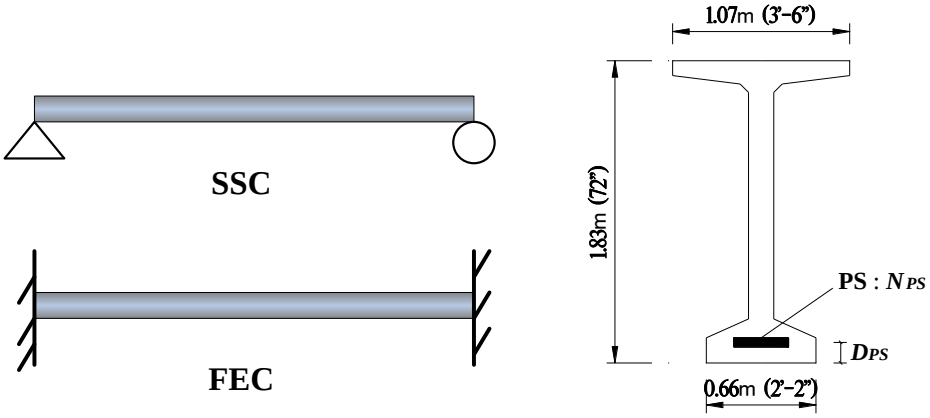

Figure 7-2. Simply supported and fix end supported girders with BT-72 section

Table 7-3. Design parameters of BT-72 section at middle span

Support condition	Span/m	f'_C (MPa / ksi)	N_{ps}	D_{ps} (m)	M_{RD} (kN.m)	M_{RT} (kN.m)
SSC	30	55 / 8	20	0.09	1.047×10^4	1.042×10^4
SSC	40	69 / 10	34	0.13	1.652×10^4	1.634×10^4
FEC	30	28 / 4	8	0.18	4.067×10^3	4.010×10^3
FEC	40	42 / 6	12	0.26	6.404×10^3	6.343×10^3

When the boundary condition change from SSC to FEC, the TU will not induce thermal force (MTU), but the nonlinear temperature gradient load (T_G) will induce MTG in statically indeterminate structure. The dead load, live load and temperature gradient load are considered in the reliability analysis. According to AASHTO LRFD, the load factor for temperature gradient, γ_{TG}, should be considered on a project-specific basis. In lieu of project-specific information to the contrary, γ_{TG} may be taken as 0.0 at the strength and extreme event limit states. The MRT under Strength I limit state from AASHTO LRFD, MRD calculated based on the design parameters (f'_C, Nps and s D_{ps}) for 30m and 40m girders under FEC are also listed in **Table 7-3**. The MRT reduced about 62% from the SSC to FEC, since both ends are restricted, the moment occurred at the fixed ends resulting in reduction of the moment at middle span. The ratio of MRD to MRT is 1.01, and β is reanalyzed to be 3.68 and 3.62 with the design parameters of 30m and 40m girders, slightly more than 3.5.

Figure 7-3 presents the reliability indices for two cases: (1) when the moment resistance of a bridge is designed as a simple support, but the actual boundary condition is a fixed end condition (DSBF); and (2) when a bridge is designed as a simple support and the actual boundary condition is a simple support condition (DSBS). The actual boundary may vary between fixed end condition and simple support condition. As in **Figure 7-3**, reliability indices of DSBF are much greater than Strength I limit state target reliability, 3.5. While the actual rotational stiffness is not fixed, results in

the Figure indicate that a bridge is designed as a simple support, but the actual boundary condition is a fixed or partially restrained is significantly conservative.

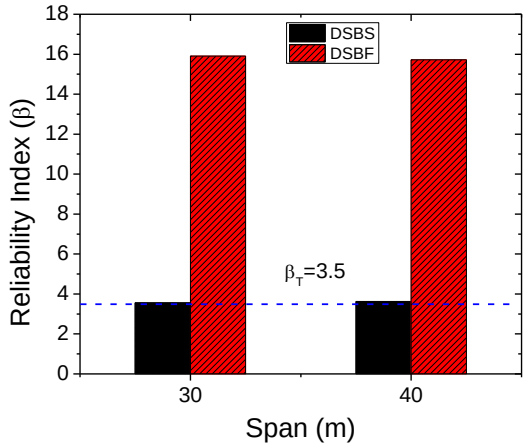

Figure 7-3. Reliability Indices with respect to Boundary Condition

Since, the boundary condition is fixed end support, the nonlinear temperature gradient load (TG) will induce thermal moment (MTG) by the following equation:

$$M_{TG} = \int \left[\sigma(y) \cdot b(y) \cdot y\right] dy = \int \left[E \cdot \alpha \cdot \Delta T(y) \cdot b(y) \cdot y\right] dy \quad (3)$$

in which ΔT(y) = the vertical temperature differential at a depth y, b(y) = the width of the girder section at a depth y, and E = the concrete modulus of elasticity. The MTG were determined using the statistics of temperature gradient in Part 1, MCS results established statistics of MTG at the mid-span section for the girder with span 30m and 40m, which are fitted to be normal distributions. According to the extreme value theory, the asymptotic distribution of the largest value of MTG (normal distribution) is of the double exponential form (Gumbel), the estimated parameters are shown in **Table 7-4**.

Table 7-4. Parameter Estimate for thermal moment (MTG) for FEC (kN.m)

Span/m	75 year					
	Domain of Attraction	The Mean □	The Standard deviation □	Domain of Attraction	The Mean □	The Standard deviation □
30	Normal	3.57×10^{2}	3.67×10^{1}	Gumbel	4.47×10^{2}	1.60×10^{1}
40	Normal	4.38×10^{2}	4.50×10^{1}	Gumbel	5.49×10^{2}	1.97×10^{1}

Considering the bending moment due to thermal load (f_{TG}) for FEC, a limit state function for Strength I limit state is:

$$g(.) = M_n - (1.25 f_{DC} + \gamma_{LL+IM} M_{LL+IM} + \gamma_{TG} M_{TG}) \quad (4)$$

In order to calibrate the load factor of γTG, thermal moments MTG under 75 year return period were adopted. And γLL+IM was assumed to be 1.25 (the same as dead load), while the M LL+IM (moment due to LL+IM) was chosen under daily traffic volume, it's value was about 80% of nominal M LL+IM under AASHTO live load model (Nowak, 1999). The moment resistance (Mn) was selected to satisfy the target reliability index (βT = 3.5) due to dead load and live load for fixed end supported girders (the limit state function recommend by AASHTO). **Figure 7-4** presents the relationship between reliability indices and load factor γ_{TG}, considering dead load, live load and temperature gradient load for PC girders with span of 30m and 40m under FEC, the reliability indices decreased almost linearly as the load factor γ_{TG} increasing. The load factor γ_{TG} should be determined to satisfy the target reliability index (βT = 3.5), the value of (β-βT)2 is calculated for different load factor γ_{TG} to obtain the optimal value, which equals 2.45 and 3.10 for the girder with span 30m and 40m, respectively. Therefore, the load factor γ_{TG} was determined as 2.45. Finally, simple support and fixed end support conditions were considered in the reliability analysis for Strength I limit state as:

$$\phi_R M_n \geq 1.25 M_{DC} + 1.75 M_{LL+IM} \quad \text{(SSC)} \quad \text{(5a)}$$

$$\phi_R M_n \geq 1.25 f_{DC} + 1.25 M_{LL+IM} + 2.45 M_{TG}) \quad \text{(FEC) (ΦR = 1.0)} \quad \text{(5b)}$$

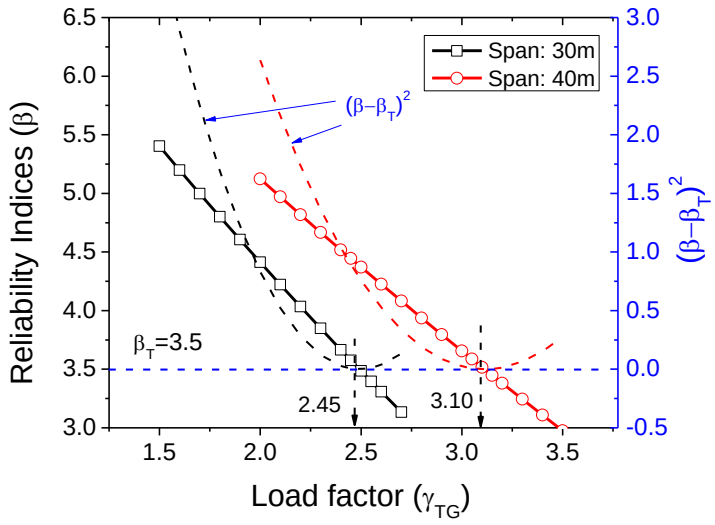

Figure 7-4. Determination of load factor γTG

8 Conclusions and Remarks

(1) A 3D structural FE accounting for the different boundary conditions was established to estimate the movement and stress under proposed temperature loading, and the accuracy was validated by filed measurements.

(2) The temperature induced movement range calculated by the method recommended in AASHTO(2012) agree well with that by FE simulation, but slightly less than the measured movement range, since the measured movement range might include other load effects, e.g. truck load.

(3) The stresses due to uniform temperature load are sensitive to boundary conditions, the normal stress change from 0.8MPa to 12MPa when the boundary condition change from simply supported condition to fixed end condition. As for the stress due to temperature gradient, there are no obvious difference for the stress distribution under proposed and AASHTO recommended positive temperature gradient, but the tensile stresses at both top slab and bottom flange under proposed negative temperature gradient are larger than stresses under AASHTO recommended one, especially at the bottom flange. The tensile stresses due to AASHTO recommended negative temperature gradient is un-conservative, even combined with other load effects, might cause cracking on the bottom of girder.

(4) Reliability analyses of AASHTO LRFD limit states were performed using Monte Carlo simulation and Rackwitz-Fiessler procedure to determine reliability index (β). Both thermal load and boundary condition have significantly influences on β, the computed reliability indices represent very low probabilities of failures, and may result in a significant overdesign. Therefore, the load factors for temperature load should be investigated to obtain a constant reliability index and to be consistent with the current AASHTO LRFD.

(5) Reliability analyses were performed to determine the partial safety factors achieving target reliability index ($\beta_T = 3.5$), and the load factors for temperature loads were recommend for AASHTO load combinations for Strength I limit state.

9 References

AASHTO (1998). *Guide Specifications for Design and Construction of Segmental Concrete Bridges*, Proposed 2nd Edition, American Association of State Highway and Transportation Officials, Washington, D.C.

AASHTO. (2012). *AASHTO LRFD bridge design specifications: (6th Ed.).* Washington, DC: American Association of State Highway and Transportation Officials.

ANSYS Theory Manual for Version 15.0, Swanson Analysis Systems, Inc., 2013.

Bojovic, A., and Velovic, N. (2014). “Rehabilitation of the Gazelle road bridge in Belgrade.” *8th Int. Conf. on Bridges in Danube Basin*, E. Petzek and R. Bancila, eds., Vieweg &Teubner Verlag, Wiesbaden, Germany, 129–138.

Dilger, W. H., Ghali, A., Chan, M., Cheung, M. S. and Maes, M. A. (1983). “Temperature stresses in composite box girder bridges,” *Journal of Structural Engineering*, vol. 109, no. 6, 1460–1478.

Duffie J.A. and Beckman W.A (2006), *Solar Engineering of Thermal Processes, 3rd Edition*, John Wiley & Son, Inc., Hoboken, New Jersey.

Elbadry, M. M. and Ghali, A. (1983). “Temperature variations in concrete bridges,” *Journal of Structural Engineering*, vol. 109, no. 10, 2355-2374.

Emanuel J.H., and Hulsey J.L. (1978), “Temperature Distributions in Composite Bridges,” *Journal of Structural Division, ASCE*, Vol. 104, No. ST1, 65-78

Emerson M. (1973), *The calculation of the distribution of temperature in bridges*, TRRL LR561 R&D Rept., Department of the Environment, Department of Transport, Crowthorne, Berkshire, England.

Fu, H. C., Ng, S. F. and Cheung, M. S. (1990). “Thermal behavior of composite bridges,” *Journal of Structural Engineering*, vol. 116, no. 12, pp. 3302-3323.

Hedegaard B., French C., and Shield C. (2013). “Investigation of Thermal Gradient Effects in the I-35W St. Anthony Falls Bridge.” *ASCE J. Bridge Eng.*, 18(9), 890–900.

Ho, D. and Liu, C.-H. (1989). “Extreme thermal loadings in highway bridges,” *Journal of Structural Engineering*, vol. 115, no. 7, 1681–1696.

Imbsen, R. A., Vandershaf, D. E., Schamber, R. A., and Nutt, R. V. (1985). “Thermal effects in concrete bridge superstructures.” *DC. NCHRP Project. Rep.*, Transportation Research Board, Washington, 12–22.

Kennedy, J., and Soliman, M. (1987). “Temperature distribution in composite bridges.” *J. Struct. Eng.,* 10.1061/(ASCE)0733-9445(1987) 113:3(475), 475–482.

Kong, B., Cai, C. S., and Kong, X. (2013). “Thermal behaviors of concrete and steel bridges after slab replacements with GFRP honeycomb sandwich panels.” *Eng. Struct.,* 56, 2041–2051.

Kong, B., Cai, C. S., and Pan, F. (2014). “Thermal Field Distributions of Girder Bridges with GFRP Panel Deck versus Concrete Deck.” ASCE *J. Bridge Eng.*, 19(11), 04014046.

Kreith F. and Kreider J.F (1978), *Principles of Solar Engineering*, McGraw-Hill, New York.

Lee, J. H. (2010). “Experimental and analytical investigations of the thermal behavior of prestressed concrete bridge girders including imperfections,” *Ph. D Dissertation*, School of Civil and Environmental Engineering, Georgia Institute of Technology, USA.

Lee, J. H. (2012). “Investigation of extreme environmental conditions and design thermal gradients during construction for prestressed concrete bridge girders,” ASCE *J. Bridge Eng.*,, vol. 17, no. 3, pp. 547–556.

Li, D., Maes, M. A., & Dilger, W. H. (2004). “Thermal design criteria for deep prestressed concrete girders based on the data from confederation bridge.” *Canadian Journal of Civil Engineering*, 31, 813-825.

Lienhard, J., and Lienhard, J. (2003). *A heat transfer textbook, 3rd Ed.,* Phlogiston Press, Cambridge, MA.

Maes, M. A., Dilger, W. H. and Ballyk, P. D. (1992). “Extreme values of thermal loading parameters in concrete bridges,” *Canadian Journal of Civil Engineering*, vol. 19, no. 6, 935–946.

Mirambell, E. and Aguado, A. (1990). “Temperature and stress distributions in concrete box girder bridges,” *Journal of Structural Engineering*, vol. 116, no. 9, 2388-2409.

Mirza, S. A., Hatzinikolas, M., and MacGregor, J. G. (1979). “Statistical descriptions of the strength of concrete.” *Journal of Structural Division, ASCE*, 105(6), 1021-1037.

Mondal, P., and DeWolf, J. T. (2007). “Development of computer-based system for the temperature monitoring of a post-tensioned segmental concrete box-girder bridge.” *Comput.-Aided Civ. Infrastruct. Eng*., 22(1), 65-77.

Moorty S. (1990), Thermal Movements in Bridges, *Ph. D Dissertation*, Department of Civil Engineering, The University of Washington, USA.

Moorty S., Roeder C.W. (1992), “Temperature-Dependent Bridge Movement,” *Journal of Structural Engineering, ASCE*, Vol. 118, No. 4, 1090-1105.

National Cooperative Highway Research Program (NCHRP 18-07). (1999). *Prestress Losses in Pretensioned High-Strength Concrete Bridge Girders*, M. K. Tadros, N. Al-Omaishi, S. J. Seguirant, J. G. Gallt. Rep 496, Transportation Research Board, Washington, D. C.

Ni Y.Q., Hua X.G., Wong K.Y., Ko J.M. (2007), “Assessment of Bridge Expansion Joints Using Long-term Displacement and Temperature Measurement,” *Journal of Performance of Constructed Facilities, ASCE*, Vol. 21, No. 2, 143-151.

Noda N., Hetnarski R.B., and Tanigawa Y. (2003), *Thermal Stresses, 2nd Edition*, Taylor & Francis, New York.

Nowak, A. S. (1995). “Calibration of LRFD Bridge Code,” *Journal of Structural Engineering, ASCE*, Vol. 121, No. 8, 1245–1251.

Nowak, A. S. (1999). *NCHRP Report 368: Calibration of LRFD Bridge Design Code*. TRB, National Research Council, Washington, D.C.

Nowak, A. S., and Szerszen, M. M. (2003). “Calibration of Design Code for Buildings (ACI 318): Part 1-Statistical Models for Resistance,” *ACI Structural Journal*, Vol. 100, No. 3, 377-382.

Nowak, A. S., Yamani, A. S., and Tabsh, S. W. (1994). “Probabilistic models for resistance of concrete bridge girders.” *ACI Structural Journal*, 91(3), 269-276.

PCI. (2003). *PCI bridge design manual (2nd ed.)*. Chicago, IL: Precast/Prestressed Concrete Institute.

Potgieter, I. C., and Gamble, W. L. (1983). “Response of highway bridges to nonlinear temperature distributions.” *Rep. No. FHWA/IL/UI-201*, Univ. of Illinois at Urbana-Champaign, Urbana-Champaign, IL.

Priestley M.J.N. (1972), Temperature Gradients in Bridges - Some Design Consideration, New Zealand Engineering, Vol. 27, Part 7, pp. 228-233.

Priestly, M. J. N. (1978). “Design of concrete bridges for temperature gradients.” *ACI J.*, 75 (5),

Rackwitz, R., and Fiessler, B. (1978). “Structural Reliability under Combined Random Load Sequences,” *Computers and Structures*, Vol. 9, 489-494.

Roberts-Wollman C., Breen J., and Cawrse J. (2002). “Measurements of Thermal Gradients and their Effects on Segmental Concrete Bridge.” *ASCE J. Bridge Eng.,* 7(3), 166–174.

Rodriguez L., Barr P., and Halling M. (2014). “Temperature Effects on a Box-Girder Integral-Abutment Bridge.” *ASCE J. Perform. Constr. Facil*., 28(3), 583–591.

Roeder C. (2003), “Proposed Design Method for Thermal Bridge Movements,” *Journal of Bridge Engineering*, Vol. 8, No. 1, 12-19.

Salawu, O. S. (1997). “Detection of structural damage through changes in frequency, a review.” Eng. Struct., 19(9), 718-723.

Shushkewich, K. W. (1998). Design of segmental bridges for thermal gradient, PCI Journal, vol. 43, no. 4, 120-137.

Soukhov D. (1994), “Two Methods for Determination of Linear Temperature Differences in Concrete Bridge with the Help of Statistical Analysis,” *Darmstadt Concrete*, Vol. 9, 193-210.

Stewart, M. G. (1997). “Time-dependent Reliability of Existing RC Structures,” *Journal of Structural Engineering, ASCE*, Vol. 123, No. 7, pp. 896-902.

Thompson, M. K., Davis, R. T. , Breen, J. E. , and Kreger, M. E. (1998). “Measured behavior of a curved precast segmental concrete bridge erected by balanced cantilevering.” *Rep. No. FHWA/TX-98/1404-2,* Univ. of Texas, Austin, TX.

Threlkeld, J. L. (1970). *Thermal environmental engineering*, Englewood Cliff, NJ: Prentice-Hall Inc.

Tong M., Tham L.G., and Au F.T.K. (2002), “Extreme Thermal Loading on Steel Bridges in Tropical Region.” *Journal of Bridge Engineering*, Vol. 7 (6), 583-593.

Westgate R., Koo K-Y, and Brownjohn J. (2015). “Effect of Solar Radiation on Suspension Bridge Performance.” ASCE *J. Bridge Eng.*, 20(5), 04014077.

Writer E.T. (2007), Field Study of Thermal Effects in Steel Plate and Box Girder Bridges, *Master’s Thesis*, The University of Houston.

Xia, Y., Xu, Y. L., Wei, Z. L., Zhu, H. P., and Zhou, X. Q. (2011). “Variation of structural vibration characteristics versus non-uniform temperature distribution.” *Eng. Struct.*, 33(1), 146–153.

Zhou, L., Xia, Y., Brownjohn, J., and Koo, K. (2015). “Temperature Analysis of a Long-Span Suspension Bridge Based on Field Monitoring and Numerical Simulation.” J. Bridge Eng., 04015027.

Zhu Z., Davidson M.T., Harik I. E., Sun L., and Sandefur K. (2015). “Effect of Superstructure Temperature Changes on Intermediate Pier Foundation Stresses in Integral Abutment Bridges.” *ASCE J. Bridge Eng.,* 20(1), 04014058.

Zuk, W. (1965), Thermal Behavior of Composite Bridges -Insulated and Uninsulated, *Highway Research Record 76*, National Research Council, pp. 231-253.